

Refractories Applications *Transactions*

Volume 1, Number 2

July/August 2005

Editorial Board

Jeffrey D. Smith, Editor, University of Missouri-Rolla, USA
Mary Lee, Assistant to the Editor, University of Missouri-Rolla, USA
William Headrick, University of Missouri-Rolla, USA
Musa Karakus, University of Missouri-Rolla, USA

Technical Referees

Esteban Aglietti, CETMC, Argentina
Richard C. Bradt, The University of Alabama, USA
Carmen Baudín, Instituto de Cerámica y Vidrio, Spain
Elena Brandaleze, Instituto Argentino de Siderurgia
Angel Caballero, Instituto de Cerámica y Vidrio, Madrid, Spain
William G. Fahrenholtz, University of Missouri-Rolla, USA
Geraldo E. Gonçalves, Magnesita S.A., Brazil
J.P. Guha, University of Missouri-Rolla, USA
Orville Hunter, Consultant, USA
William E. Lee, University of Sheffield, UK
Li Nan, Wuhan University of Sci. & Tech., China
George Oprea, The University of British Columbia, Canada
Victor C. Pandolfelli, Universidade Federal de São Carlos, Brazil
Christopher Parr, Lafarge Aluminates, France
Jacques Poirier, Polytech, Orleans, France
Michel Rigaud, Ecole Polytechnique, Canada
Charles Semler, Semler Materials Services, USA
Mark Stett, Consultant, USA
Raul Topolevsky, Siderar, Argentina

All submissions should be sent to:

Mary Lee, Assistant to the Editor
Refractories Applications Transactions
University of Missouri-Rolla
Materials Science and Engineering Dept.
223 McNutt Hall
1870 Miner Circle Drive
Rolla, MO 65409-0330

Phone: (573) 341-6561
Fax: (573) 341-6934
E-mail: leem@umr.edu

For author guidelines please see those listed on the *Journal of the American Ceramic Society* website: <http://www.ceramics.org/publications/journal/authorinstructions.asp>

File Formats

Text: Microsoft Word.

Graphics: JPEG, TIFF or EPS created from supported applications, PowerPoint, Acrobat PDF (PDF format is acceptable for review purposes only)

Microsoft Word with embedded graphics.

Compression Software: WinZip (PC) or Stuffit (Macintosh)

Resolution of graphics files must be at least 300 dpi for halftones, 600 dpi for lettering, and 1200 dpi for line art.

Oxidation of ZrB₂-SiC Ceramics Under Atmospheric and Reentry Conditions

A. Chamberlain*, W. Fahrenholtz*, and G. Hilmas* and D. Ellerby**

*Materials Science and Engineering, University of Missouri-Rolla, Rolla, MO 65409

**NASA Ames Research Center, Moffett Field, CA 94035

Abstract

The oxidation behavior of ZrB₂-based ceramics was studied using thermal gravimetric analysis and arc jet testing. Commercially available powders were used to prepare ZrB₂ ceramics containing 0, 10, 20, and 30 volume percent SiC particulates. Thermal gravimetric analysis was used to characterize oxidation behavior by heating at 10°C/min to 1500°C in air. Weight gains ranged from 0.05 mg/mm² for pure ZrB₂ to 0.01 mg/mm² for ZrB₂ containing 30% SiC. A thin (<5 μm) layer of borosilicate glass was found on the surface of specimens containing SiC. For specimens containing 10 or 20 vol.% SiC, the ZrB₂ immediately below the glassy layer was devoid of SiC. Thermodynamic calculations showed that SiC could be removed as SiO and CO without oxidizing ZrB₂ at 1500°C. The oxidation behavior of two specimens containing 30% SiC was also examined under atmospheric re-entry conditions by arc jet testing. At a heat flux of 350 W/cm², the surface temperature increased to ~1700°C after ~30 seconds. An average mass loss of 0.8% was measured after 600 seconds. After exposure, a layer of ZrO₂, a partially oxidized layer, and a SiC depletion layer formed on the surface of the specimens. The thermodynamic model developed from the experimental results is the first step toward understanding the fundamental oxidation mechanisms, and, in turn, designing additives or coatings that will reduce the oxidation rate of ZrB₂-based ceramics used in thermal protection applications.

Introduction

Refractory borides and carbides such as ZrB₂, ZrC, HfB₂, HfC, and TaC possess melting temperatures greater than 3000°C making them candidates for structural applications at temperatures above 1800°C.¹ Of those ultra high temperature ceramics (UHTCs), ZrB₂ has the lowest theoretical density, 6.09 g/cm³, which makes it an attractive material for aerospace applications such as leading edges on hypersonic vehicles.^{2,3} Other current or potential applications for UHTCs include molten metal crucibles and high temperature electrodes.⁴⁻⁷ Along with its high melting temperature, ZrB₂ has excellent thermal shock resistance because of its high thermal conductivity, which ranges from 65 to 135 W/m•K.⁸ Pure ZrB₂ is resistant to oxidation up to 1000°C due to the formation of a passive layer of B₂O₃. Above 1000°C, oxidation resistance of pure ZrB₂ is poor due to volatilization of B₂O₃, which results in formation of a porous, non-protective ZrO₂ layer. Zirconium diboride ceramics containing SiC have improved oxidation resistance between 1000°C and 1800°C due to the formation of less volatile silica-containing scales.⁹

Interest in UHTCs has increased significantly in recent years because of the drive to produce thermal protection systems (TPS) and other components for hypersonic aerospace vehicles.³ Current TPS, such as the SiC-coated carbon-carbon composites used on the leading edge of the space shuttle orbiter, lack the necessary oxidation resistance for use above 1650°C in air. Improvements in coating technology, primarily SiC coatings on carbon-carbon composites, could improve the oxidation resistance and extend the operational temperatures for carbon-based TPS materials. However, pure SiC coatings have an inherent limit due to the transition from passive to active oxidation that occurs below 1700°C for typical Earth re-entry conditions. Also, the ability of ceramic coatings on carbon-carbon materials to endure thermal cycling will always be questionable because the large mismatch in the coefficients of thermal expansion between the coating (~3 ppm/°C for SiC) and the underlying composite (essentially 0) leads to microcracking, which exposes the matrix to the oxidizing environment.

The current space shuttle orbiter has a blunt body design that limits the maximum surface temperature on the leading edges of the orbiter to ~1650°C.¹¹ During re-entry, the surface temperature is proportional to the inverse square root of the body radius (e.g., the leading edge radius of the orbiter). Therefore, the larger the radius or the more blunt the body, the lower the surface temperature. Unfortunately, large, blunt leading edges reduce vehicle maneuverability. Most modern designs for hypersonic vehicles incorporate sharp leading edges to increase aerodynamic performance, but require materials capable of operating in oxidizing atmospheres at temperatures over 1700°C.¹² For example, predicted steady state surface temperatures for extended flights at Mach 10 (the speed reached for a few seconds in a recent NASA flight test of the X43A scramjet*) are ~2100°C.¹⁰ Studies in the 1960's and 70's showed that Zr- and Hf-based diborides have sufficient strength and oxidation resistance at high temperature for leading edge applications.¹³ Additives such as graphite and SiC were found to improve densification behavior, thermal shock resistance, and oxidation resistance of the diborides.^{14,15} Addition of twenty volume percent of SiC particulates improved the oxidation resistance of the ZrB₂ by promoting the formation of borosilicate layer with low oxygen permeability leading to passive oxidation kinetics. Additions of TaSi₂ and TaB₂ to ZrB₂-20 vol.% SiC composites have been shown to further improve oxidation resistance between 1200° and 1400°C.^{16,17} During oxidation, these compounds form Ta₂O₅, which promotes phase separation in the glassy layer and is thought to reduce oxygen transport rates.

The purpose of this paper is to compare the oxidation behavior of ZrB₂ ceramics containing 0 to 30 volume percent SiC in flowing air and to evaluate the performance of ZrB₂-30% SiC under simulated re-entry conditions in arc jet testing.

Procedure

Composite Processing

Billets of ZrB₂ and ZrB₂-SiC were prepared from commercial ZrB₂ (Grade B, H.C. Starck, Newton, MA, ~2 μm) and SiC (UF-10, H.C. Starck, Newton, MA, ~0.7 μm). Powders were batched to produce either pure ZrB₂ (no SiC addition) or ZrB₂ containing 10, 20, or 30 volume percent SiC particulates. After batching, powders were attrition milled (Model HD-01, Union Process, Akron, OH) to reduce particle size and promote uniform mixing. Milling was accomplished in a 750 ml polymer lined bucket charged with 3000 grams of WC media, 131 to 152 grams of powder (Table I), and 250 ml of hexane. The mixture was milled for 2 hours at 600 rpm using a polymer-coated spindle with WC agitator arms. After milling, the solvent was removed by rotary evaporation (Rotavapor R-124, Buchi, Flawil, Switzerland) to minimize segregation during drying.

Milled powders were uniaxially hot pressed (HP-3060, Thermal Technology, Santa Rosa, CA) in a boron nitride coated graphite die. The precise heating schedule has been described elsewhere.¹⁸ Samples were pressed at 1900°C for 45 minutes at a pressure of 32 MPa (~5000 psi). After densification, the bulk density of hot pressed billets was determined using the Archimedes' method with water as the immersing medium. The relative density of each composition was determined by dividing the bulk density by the true density. For each composition, the true density was estimated by grinding a small (~5 g) sample of the billet to -325 mesh and then measuring the powder density using helium pycnometry.

Oxidation Studies

Atmospheric oxidation studies were conducted using thermal gravimetric analysis (TGA). Sample size was approximately 1 mm x 1.5 mm x 1.5 mm. Dimensions were measured to ± 0.01 mm to calculate the surface area of each test coupon. Weight change was measured under flowing air at a ramp rate of 10°C up to 1500°C without an isothermal hold. Cross sections of oxidized samples were examined using scanning electron microscopy (SEM; S570, Hitachi, Tokyo). Chemical analysis was performed using electron dispersive spectroscopy (EDS; AAT, X-ray Optics, Gainesville, FL).

The behavior of ZrB₂-30%SiC was also studied under simulated reentry conditions using arc jet testing conducted in the 60 MW Interactive Heating Facility at the NASA-Ames Research Center. Two cylindrical test coupons, approximately 2.5 cm in diameter, were exposed to a heat flux of 350 W/cm² with a stagnation pressure of 0.07 atm. The heat flux was referenced to a 7.63 cm diameter Cu hemisphere (Gardon gauge). The exact heat flux to the surface of the model was uncertain due to differences in shape and surface properties (e.g., catalytic activity in the plasma) between the model and the gauge. The surface temperature of the test specimens was monitored using both a one-color pyrometer (M90V, Mikron, Oakland, NJ) and a two-color pyrometer (M190R2, Mikron, Oakland, NJ). Post-test characterization of surface oxidation and the underlying microstructure was performed using SEM and EDS.

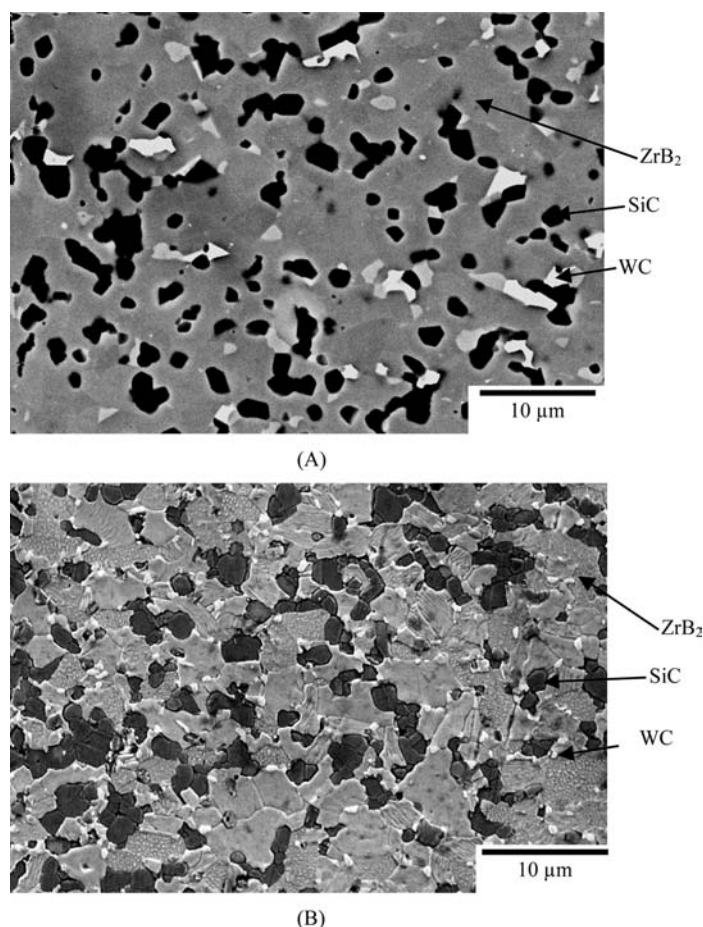


Fig. 1. SEM micrographs showing a polished cross section of ZrB₂-20% SiC and (B) a polished and thermally etched cross section of ZrB₂-30%SiC, both hot pressed at 1900°C.

Results and Discussion

Density and Microstructure

The bulk densities of hot pressed billets ranged from 6.26 g/cm³ for pure ZrB₂ to 5.43 g/cm³ for ZrB₂-30% SiC (Table II), depending on SiC content. These density values correspond to relative densities of >99% for the pure ZrB₂ and ZrB₂ containing 20 or 30 vol.% SiC. The relative density of ZrB₂-10% SiC was ~93%. Examination by SEM/EDS showed that the SiC was well dispersed in the ZrB₂ matrix (Fig. 1A) and that the average grain size was less than 5 μm (Fig. 1B). In addition, ~2 vol.% WC was found. The WC impurities were incorporated during the attrition milling

Table I. Compositions for the batches used to produce ZrB₂-SiC.

SiC Content (vol%)	ZrB ₂ (g)	SiC (g)	Total Batch (g)
0	152	0	152
10	137	8	145
20	122	16	138
30	107	24	131

Table II. Bulk and relative density for hot pressed ZrB₂-SiC.

SiC Content (vol%)	Bulk Density (g/cm ³)	Powder Density (g/cm ³)	Relative Density (%)
0	6.26	6.27	>99
10	5.54	5.94	~93
20	5.72	5.74	>99
30	5.43	5.46	>99

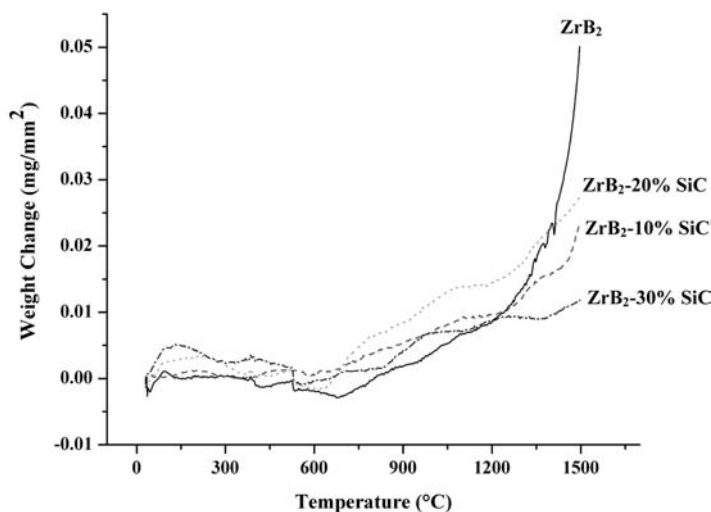


Fig. 2. Weight gain as a function of temperature for hot pressed ZrB_2 and ZrB_2 -SiC.

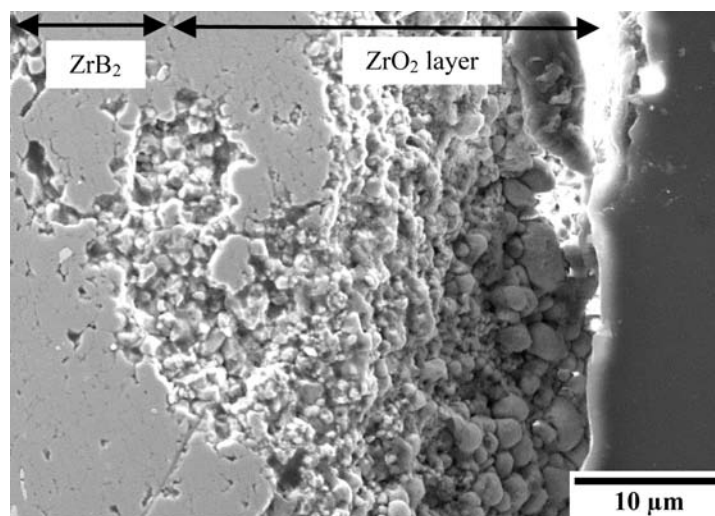


Fig. 3. SEM micrograph of the cross section of pure ZrB_2 after oxidation at $1500^\circ C$.

step due to the use of WC milling media. Examination of ZrB_2 , ZrB_2 -20% SiC, and ZrB_2 -30% SiC specimens using SEM confirmed that these compositions were fully dense (no apparent porosity). Based on Archimedes' density measurements and SEM observations, it was determined that the ZrB_2 -10% SiC specimen contained ~7 vol.% closed porosity.

Furnace Oxidation

Using TGA, the change in mass as a function of temperature was measured up to $1500^\circ C$ (Fig. 2). Pure ZrB_2 and all of the ZrB_2 -SiC specimens had similar mass gain characteristics up to $1200^\circ C$. In this temperature regime, the oxidation rate was relatively slow and resulted in mass gains of ~ 0.01 mg/mm^2 for all materials. Isothermal studies (not shown) revealed parabolic kinetics indicative of passive oxidation through a stable, protective oxide film that was increasing in thickness as exposure time increased. For pure ZrB_2 , protection is due to the formation of B_2O_3 .¹⁹ Above $1200^\circ C$, the mass gain for pure ZrB_2 was considerably greater than for the other specimens. In addition, the rate of mass gain, as indicated by the slope of the TGA curve, increased as temperature increased. Analysis

Table III. Normalized mass gains and oxide layer thicknesses for ZrB_2 -SiC during TGA at $10^\circ C/min$ to $1500^\circ C$ in air.

SiC Content (vol%)	Mass Gain/Surface Area (mg/mm^2)	Oxide Thickness (μm)
0	0.05	60
10	0.02	4.2
20	0.03	1.9
30	0.01	1.5

of the oxide layers formed on pure ZrB_2 by heating to $1500^\circ C$ (Fig. 3) using SEM/EDS showed that the reaction layer was ~ 60 μm thick. For pure ZrB_2 , volatilization of B_2O_3 in this temperature range leaves a porous, non-protective layer of ZrO_2 behind as the only oxide reaction product. The normalized mass gain (total mass gain divided by surface area calculated from the dimensions of the rectangular prism) for the ZrB_2 specimen heated to $1500^\circ C$ was 0.05 mg/mm^2 (Table III). The slope of the TGA curve and additional isothermal experiments indicate that ZrB_2 undergoes active oxidation in this temperature regime, as reported in other studies. No evidence of WC or W-containing phases was found in the oxidized portion of the ZrB_2 . Presumably, WC formed CO (or CO_2) and one or more volatile W-oxides upon exposure resulting in complete removal from the oxidized layer. Its presence did not seem to have a significant effect on the overall oxidation process and it was disregarded for the other compositions.

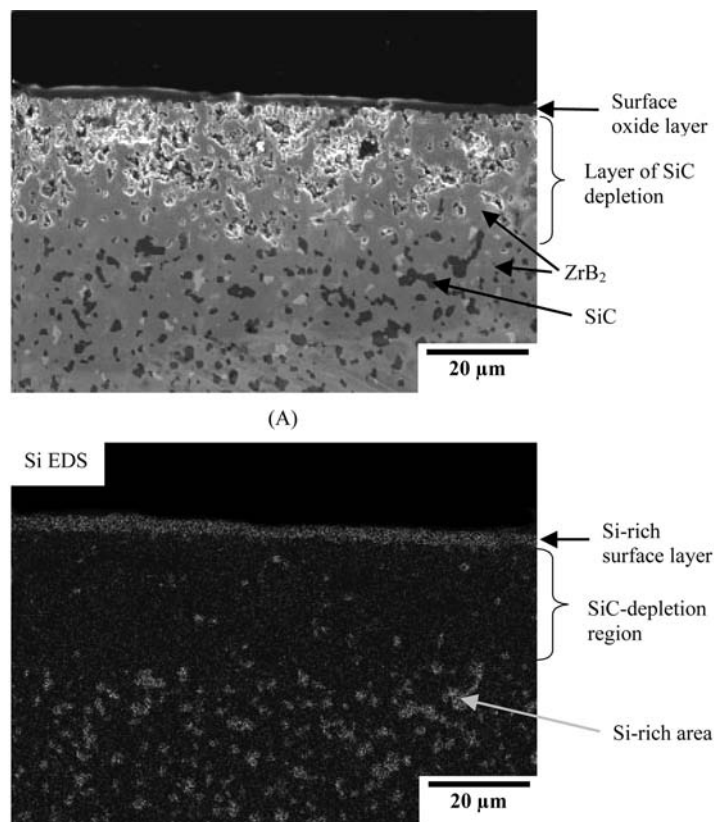


Fig. 4. (A) SEM image of the oxide layer and depletion layer formed by oxidation of ZrB_2 -20% SiC at $1500^\circ C$ in air and (B) EDS map of silicon verifying the reduction of Si content in the depletion layer (light gray indicates the presence of Si).

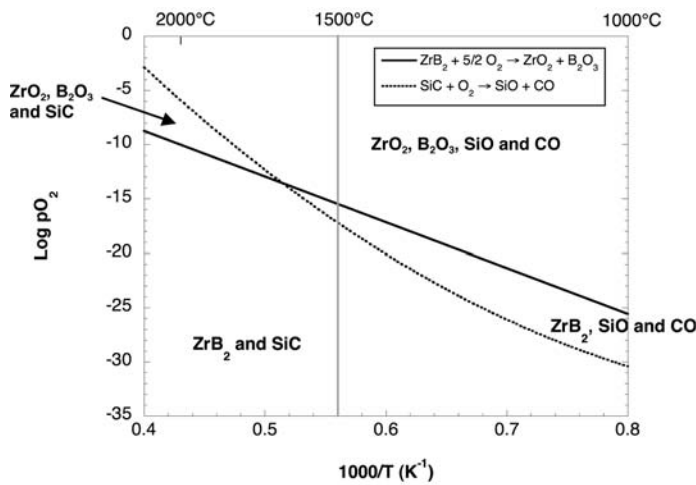
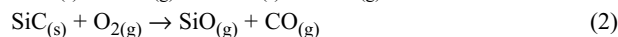
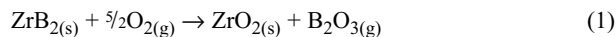


Fig. 5. Phase stability diagram for ZrB₂-SiC plus O₂ with labels designating the stable phases in each region. The vertical line at 1500°C crosses a p_{O₂} region where ZrB₂ is stable, but SiC is not.

For ZrB₂ containing SiC, the total mass gains and the rates of mass gain above 1200°C were less than for pure ZrB₂. The mass gains loosely correlate to SiC content, with ZrB₂-30% SiC gaining the least mass (0.01 mg/mm²) during the TGA experiment (Table III). Weight gains and layer thicknesses for the 10% SiC material did not follow the trends of the other specimens due to the presence of porosity in the ZrB₂-10% SiC. The enhanced protection of the SiC-containing specimens was due to the formation of a borosilicate scale rather than the B₂O₃ scale formed on ZrB₂. For the borosilicate scale, volatilization of B₂O₃ from the surface leaves behind a cohesive silica-rich layer still capable of providing passive oxidation resistance.¹⁵ Examination of a cross section of the ZrB₂-20% SiC specimen after oxidation at 1500°C in air showed that the surface oxide layer was ~2 μm thick (Fig. 4A). For specimens containing 10, 20, or 30 vol.% SiC, the layer just below the oxide scale was ZrB₂ that was depleted of SiC. Mapping of Si concentration using EDS (Fig. 4B) showed that the surface layer was Si-rich, presumably silicate or borosilicate glass. The bulk of the specimen had Si-rich regions corresponding to the SiC particulates. This analysis revealed that most of the Si had been removed from the region between the oxide layer and the bulk ZrB₂-SiC. The selective removal of SiC from this region suggests that active oxidation of SiC had occurred without significant oxidation of ZrB₂. Justification for this assertion is provided by the thermodynamic calculations below.

At the interface between the depletion layer (assumed to be ZrB₂) and the unaltered ZrB₂-SiC material, SiC is oxidized and removed, but ZrB₂ is stable. Upon its initial exposure to oxygen, ZrB₂ would be expected to form B₂O₃ vapor and solid ZrO₂ as described by Reaction 1. Similarly, the initial response of SiC can be described by Reaction 2.



The choice of phases is based on phases observed at the interface between the depletion layer and the unaltered ZrB₂-SiC after oxidation at ~1500°C. Any B₂O₃ formed would be expected to volatilize rapidly at 1500°C. Likewise, SiC reacts to form SiO and CO with SiO₂ only forming near the outer surface depletion layer near the surface of the specimen (i.e., SiO₂ is not observed in contact with ZrB₂-SiC under these conditions). Using Gibbs' free energy of formation (ΔG_f) data from standard reference tables,²⁰ the Gibbs' free energy of reaction (ΔG_{rxn}) for Reactions 1 and 2 can be calculated as a function of temperature. At

1500°C, ΔG_{rxn} is -1246.2 kJ for Reaction 1 and -454.7 kJ for Reaction 2. By equating these values to expressions for the equilibrium constant (Equation 3) for each reaction (Equations 4 and 5), the partial pressure of oxygen (p_{O₂}) can be calculated as a function of temperature for Reactions 1 and 2.

$$\Delta G_{\text{rxn}} = -RT \ln K_{\text{eq}} \quad (3)$$

Where: R is the ideal gas constant (8.314 J/mole•K)

T is the absolute temperature

K_{eq} is the equilibrium constant

$$K_{\text{eq, ZrB}_2} = \frac{P_{\text{B}_2\text{O}_3}}{(P_{\text{O}_2})^{5/2}} \quad (4)$$



(A)

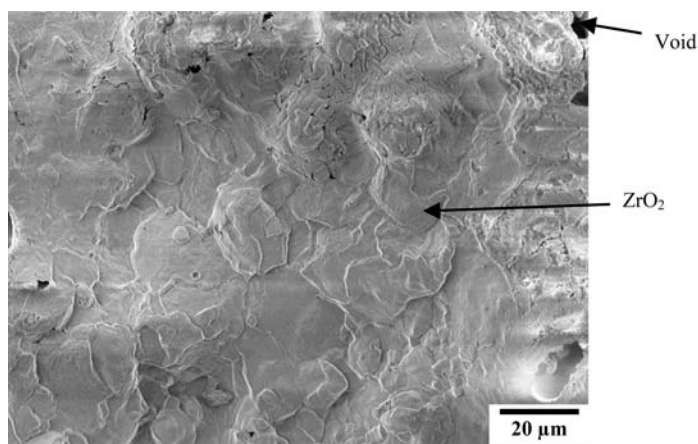


(B)

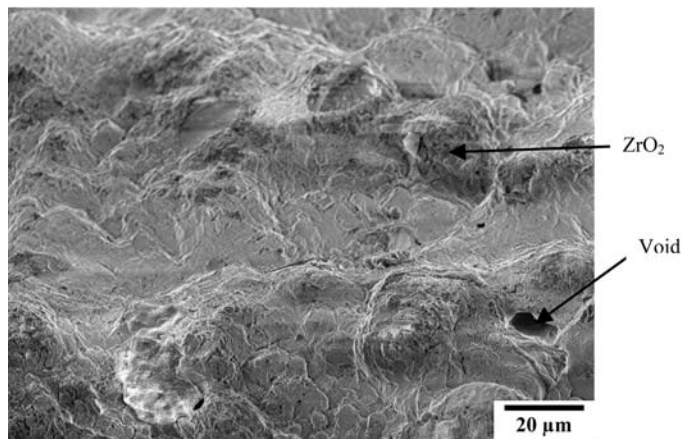
Fig. 6. The surface of a ZrB₂-30%SiC specimen (A) before and (B) after arc jet testing. Specimen diameter is 1 inch.

$$K_{\text{eq, SiC}} = \frac{p_{\text{SiO}} \cdot p_{\text{CO}}}{p_{\text{O}_2}} \quad (5)$$

To calculate $K_{\text{eq, ZrB}_2}$, $p_{\text{B}_2\text{O}_3}$ was assumed to be the equilibrium vapor pressure of B_2O_3 that can be calculated from available Gibbs' free energy data for the liquid and vapor phases.²⁰ The determination of p_{SiO} and p_{CO} was more complex. In the temperature range of 1000 to 2000 K, p_{SiO} and p_{CO} were calculated from a SiC volatility diagram prepared as part of a broader study of the thermodynamics of ZrB_2 -SiC oxidation. A ZrB_2 -SiC phase stability diagram in the temperature range of 1000°C to 2000°C was calculated (Fig. 5) by plotting the equilibrium p_{O_2} for Reactions 1 and 2 as a function of temperature. At any temperature, ZrB_2 and SiC are stable at p_{O_2} values below both lines. Between 1000°C and ~1700°C, temperature- p_{O_2} combinations are possible for stability of ZrB_2 , but oxidation of SiC. The conditions for active oxidation of SiC, but stability of ZrB_2 are described by the area above the equilibrium p_{O_2} for the oxidation of SiC (dashed black line on Fig. 5), but below the equilibrium p_{O_2} for oxidation of ZrB_2 (solid black line on Fig. 5). At 1500°C, the equilibrium p_{O_2} for SiC oxidation is $\sim 10^{-17}$ while the equilibrium p_{O_2} for ZrB_2 oxidation is 10^{-15} . During oxidation, the p_{O_2} in the depletion layer, including the interface between the depletion layer and the unaltered ZrB_2 -SiC, would be set by



(A)



(B)

Fig. 7. SEM images of the surface of ZrB_2 -30%SiC after arc jet testing from (A) near the center of the specimen and (B) near the edge of the specimen.

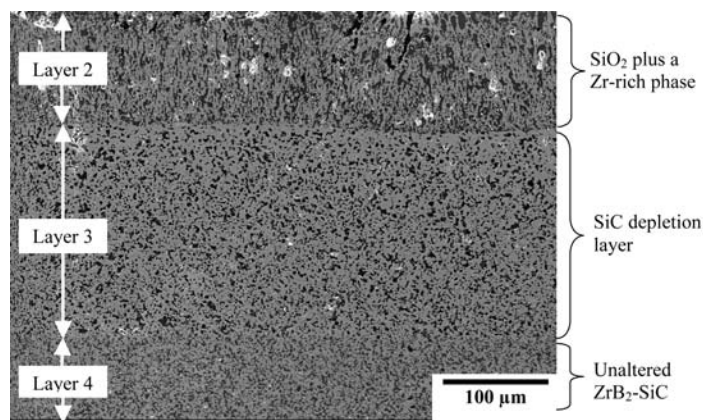


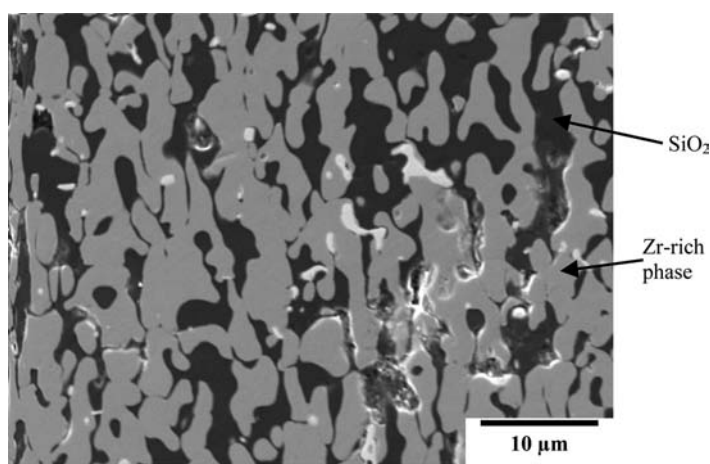
Fig. 8. Polished cross section of a ZrB_2 -30%SiC specimen showing three of the four layers formed during arc-jet testing.

the oxidation of SiC (i.e., the equilibrium among CO , SiO , SiC , and O_2) thereby protecting ZrB_2 from attack. Formation of SiO_2 would be favored only at the outer surface of the specimen where SiO could react with O_2 from the flowing air atmosphere. After formation of the initial scale, the rate of condensation of SiO to SiO_2 is likely controlled by the diffusion of O_2 through the SiO_2 scale resulting in the parabolic oxidation kinetics observed in other studies.¹⁹

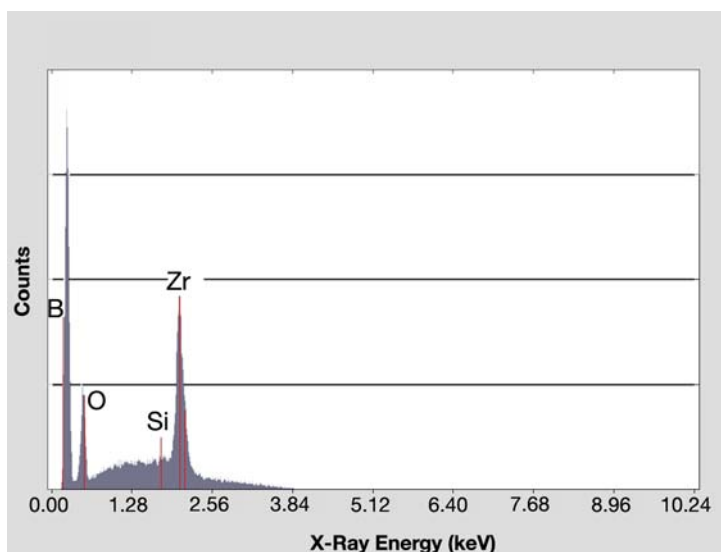
Arc Jet Testing

The performance of two ZrB_2 -30% SiC specimens was evaluated in simulated atmospheric re-entry conditions using arc jet testing. During operation, an arc is struck between electrodes in a column. Gas flows through the arc column, is heated, and then expands through a nozzle. The gas convectively heats the specimen with typical stream enthalpies on the order of mega-Joules per kg (MJ/kg) of gas. A stagnation heat flux of $\sim 350 \text{ W/cm}^2$ was measured using the Cu Gardon gauge. Images of the surfaces of the ZrB_2 -SiC specimens before and after testing are shown in Fig. 6. During exposure, the surface temperature of the specimen, as monitored by a two color optical pyrometer, increased from room temperature to $\sim 1700^\circ\text{C}$ within about 30 seconds. The surface temperature increased slowly during the remaining 570 seconds of the test, approaching 1800°C after 600 seconds. The two specimens lost $\sim 0.8 \text{ wt.}\%$ during testing due to volatilization of reaction products. Most likely, high vapor pressure species such as B_2O_3 , B_2O_2 , B_2O , and SiO were evolved during testing. After exposure (Fig. 6B), the surface appeared oxidized. Examination by SEM (Fig. 7) and EDS suggests that the surface layer was primarily composed of ZrO_2 . The surface layer appears dense with the exception of a few, relatively large ($\sim 15 \mu\text{m}$) voids. These voids are more numerous near the center of the specimen than near the edge, possibly due to a temperature gradient across the surface. Evaluation of Hf-based UHTCs has shown formation of similar voids in the surface oxide layer, although the number of voids appears greater in the Hf-based specimens.^{21,22} The Hf-based materials were tested under nominally identical conditions, but had a higher surface temperature due to differences in emissivity. The higher temperatures may have caused the formation of additional voids since they are thought to allow gaseous products formed in the depletion layer to escape.

After testing, arc jet specimens were sectioned and polished for SEM/EDS (Fig. 8). Analysis revealed the presence of four distinct layers, in contrast to the three distinct layers reported for Hf-based materials.²² The outer layer (not shown in Fig. 8) was $\sim 10 \mu\text{m}$ thick and composed of ZrO_2 , as had been observed in Fig. 7. Beneath the ZrO_2 was a layer ~ 100



(A)



(B)

Fig. 9. (A) An SEM image of layer 2 showing two phases, a silica-rich phase and a Zr-rich phase; and (B) an EDS spectrum of the zirconium-rich phase showing the presence of oxygen and boron with little or no silicon.

μm thick (Layer 2) that was not reported for Hf-based materials. From Fig. 8, it appears that this layer may have been molten under the test conditions. Further analysis of Layer 2 (Fig. 9) showed that it consisted of a SiO₂-rich phase (dark phase) and a Zr-rich phase (light phase). Compositional analysis by EDS showed that the Zr-rich phase was composed of mainly Zr and B, but that it also contained some O. Apparently, this is a transitional region between fully oxidized ZrO₂ and the underlying SiC-depletion region (layer 3). Thermodynamically, this would be possible if the temperature of the specimen was above ~1750°C, the temperature where the stability fields on Fig. 5 converge near the left side of Fig. 5. The fourth layer is the unaltered ZrB₂-SiC.

The interface between Layers 2 and 3 is shown at higher magnification in Fig. 10. This image shows a sharp transition from a SiO₂ containing layer to the SiC depletion layer. As with the furnace oxidation specimens, active oxidation of SiC occurred at the interface between the depletion layer and ZrB₂-SiC. Apparently, SiO condenses to form SiO₂ at the interface shown in Fig. 10 between the depletion layer and the partially oxidized layer. Based on the measured surface temperatures, the observed

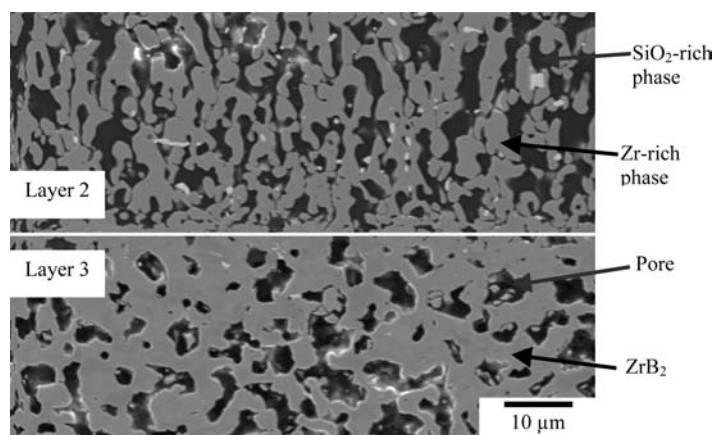


Fig. 10. An image of the interface between layers 2 and 3 in the arc jet specimen.

layer structure may be indicative of a slight, but significant temperature gradient through this section.

Summary

Specimens of dense ZrB₂ containing 0, 10, 20, or 30 volume percent SiC particulates were produced by hot pressing. Up to ~1200°C, the furnace oxidation behavior of pure ZrB₂ and ZrB₂-SiC were similar due to the formation of a protective B₂O₃ layer on the surface. At higher temperatures, B₂O₃ vaporization resulted in an increased oxidation rate for the pure ZrB₂ specimen. The rate of oxidation of specimens containing SiC was lower due to the incorporation of SiO₂ into the protective layer. The total mass gain during heating to 1500°C in air decreased from 0.05 mg/mm² for ZrB₂ to 0.01 mg/mm² for ZrB₂-30% SiC. Examination of the cross section of oxidized specimens revealed the presence of a SiC depletion region between the protective oxide and the unaltered ZrB₂-SiC. The conditions required to promote the oxidation of SiC, but the stability of ZrB₂ were defined using a phase stability diagram. Two ZrB₂-30% SiC specimens were evaluated under simulated re-entry conditions using arc jet testing. A layer of ZrO₂ ~10 micro-meters thick formed on the surface of the specimens. Below the ZrO₂ was a layer containing a mixture of SiO₂ and Zr-rich phases. The arc jet specimens also contained a SiC depletion layer. Studies are underway to apply these findings to design additives or coatings that will improve the oxidation resistance of ZrB₂-based materials for thermal protection applications.

Acknowledgements

This work was supported by the Air Force Office of Scientific Research under Grant Number F49620-03-1-0072. Financial support for ALC was also provided by a Graduate Assistance in Areas of National Need (GAANN) Fellowship sponsored by the Department of Education. The authors would like to thank Ms. Michelle Schaeffler for technical assistance.

References

- R. Telle, L.S. Sigl, and K. Takagi, "Boride-Based Hard Materials," pp. 802-945 in Handbook of Ceramic Hard Materials, edited by R. Riedel, Wiley-VCH, Weinheim, 2000.
- D.M. Van Wie, D.G. Drewry, Jr., D.E. King, and C.M. Hudson, "The Hypersonic Environment: Required Operating Conditions and Design Challenges," *J. of Mater. Sci.*, **39**[19] 5915-5924 (2004).
- M.M. Opeka, I.G. Talmy, and J.A. Zaykoski, "Oxidation-Based Materials Selection for 2000°C+ Hypersonic Aerosurfaces: Theoretical Considerations and Historical Experience," *J. of Mater. Sci.*, **39**[19] 5887-5904 (2004).
- S. Kinoshita, Y. Miyagishi, and Y. Ono, "Application of Zirconium Diboride Materials to Waste Melting Furnaces," pp 205-208 in the Proceedings of UNITECR 2003 Congress, 8th Biennial Worldwide Conference on Refractories, Osaka, Japan, October 19-22, 2003.
- C. Mroz, "Zirconium Diboride," *American Ceramic Society Bulletin*, **73**[6] 141-42 (1994).

- ⁶ R. Tanaka, "Research and Development of Ultra-High Temperature Materials in Japan," *Materials at High Temperature*, **17**[4] 457-464 (2000).
- ⁷ N. Kaji, H. Shikano, and I. Tanaka, "Development of ZrB₂-Graphite Protective Sleeve for Submerged Nozzle," *Taikabutsu Overseas*, **14**[2] 39-43 (1992).
- ⁸ R.A. Cutler, "Engineering Properties of Borides," pp. 787-803 in *Ceramics and Glasses, Engineered Materials Handbook*, Vol. 4, ed. S.J. Schneider. ASM International, Materials Park, OH, 1992.
- ⁹ C. Bartuli, T. Valente, and M. Tului, "Plasma Spray Deposition and High Temperature Characterization of ZrB₂-SiC Protective Coatings," *Surface and Coatings Technology*, 155 260-273 (2002).
- ¹⁰ S.P. Walker and B.J. Sullivan, "Sharp Refractory Composite Leading Edges on Hypersonic Vehicles," AIAA-6915, 12th AIAA International Space Planes and Hypersonic Systems and Technologies Conference, Norfolk, VA, December 15-19, 2003.
- ¹¹ D.S. Richerson, *Modern Ceramic Engineering*, Marcel Dekkar, New York, 1992.
- ¹² P. Kolodziej, "Aerothermal Performance Constraints for Hypervelocity Small Radius Unswept Leading Edges and Nosedips," NASA Technical Memorandum 112204, July 1997.
- ¹³ L. Kaufmann and H. Nesor, "Stability Characterization of Refractory Materials under High Velocity Atmospheric Flight Conditions, Part I, Vol. I, Summary," Technical Report No. AMFL-TR-69-84, Air Force Materials Laboratory, Wright-Patterson Air Base, OH (1970).
- ¹⁴ Edward Clougherty, R. Hill, W. Rhodes, and E. Peters, "Research and Development of Refractory Oxidation-Resistant Diborides, Part II, Vol. II: Processing and Characterization," Technical Report No. AFML-TR-68-190, Air Force Materials Laboratory, Wright-Patterson Air Base, OH, (1969).
- ¹⁵ W.C. Tripp, H.H. Davis, H.C. Graham, "Effect of a SiC Addition on the Oxidation of ZrB₂," *Am. Ceram. Soc. Bull.*, **52**[8] 612-16 (1973).
- ¹⁶ E. Opila, S. Levine, and J. Lorincz, "Oxidation of ZrB₂- and HfB₂-Based Ultra-High Temperature Ceramics: Effect of Ta additions," *J. Mater. Sci.*, **39**[19] 5969-5977 (2004).
- ¹⁷ I.G. Talmy, J.A. Zaykoski, M.M. Opeka, and S. Dallek, "Oxidation of ZrB₂ Ceramics Modified with SiC and Group IV-VI Transition Metal Borides," pp. 144-158 in *High Temperature Corrosion and Materials Chemistry III*, ed. by E. J. Opila, M. J. McNallan, D. A. Shores, and D. A. Shifler, The Electrochemical Society, Pennington, NJ (2001).
- ¹⁸ A.L. Chamberlain, W.G. Fahrenholtz, G.E. Hilmas, and D.T. Ellerby, "High Strength ZrB₂-Based Ceramics," *J. Am. Ceram. Soc.*, **87**[6] 1170-1172 (2004).
- ¹⁹ W.C. Trip, H.H. Davis, H.C. Graham, "Effect of a SiC Addition on the Oxidation of ZrB₂," *Ceram. Bull.*, **52**[8] 612-16 (1973).
- ²⁰ M.W. Chase, Jr., NIST-JANAF Thermochemical Tables, Fourth Edition, Journal of Physical and Chemical Reference Data, Monograph 9, American Institute for Physics, Woodbury, NY (1998).
- ²¹ M. Gasch, D. Ellerby, E. Irby, S. Beckman, M. Gusman, and S. Johnson, "Processing and Properties and Arc Jet Oxidation of Hafnium Diboride/Silicon Carbide Ultra High Temperature Ceramics," *J. Mater. Sci.*, **39**[19] 5925-5937 (2004).
- ²² J.D. Bull, and D.J Rasky, "Stability Characterization of Diboride Composites Under High Velocity Atmospheric Flight Conditions," 24th International SAMPE Technical Conference, Oct. 20-22, 1992.